Reaction Chemistry & Engineering

ROYAL SOCIETY OF CHEMISTRY

PAPER

View Article Online
View Journal | View Issue

Check for updates

Cite this: *React. Chem. Eng.*, 2023, **8**, 661

A new process for the recovery of palladium from a spent Pd/TiO_2 catalyst through a combination of mild acidic leaching and photodeposition on ZnO nanoparticles†

Marica Muscetta, *[a] Giulio Pota,[a] Giuseppe Vitiello, [a] Samar Al Jitan,[b] Giovanni Palmisano,[b] Roberto Andreozzi,[a] Raffaele Marotta[a] and Ilaria Di Somma*[c]

Received 15th June 2022,
Accepted 18th November 2022

DOI: 10.1039/d2re00240j

rsc.li/reaction-engineering

Currently, palladium represents an expensive and scarce element in the Earth's crust, with the mineral resources of platinum group metals (PGMs) predominately localized in South Africa and Russia. The growing demand for this material necessitates the development of suitable strategies to recover it from end-of-life devices. The recovery of palladium by combining leaching and sacrificial photocatalytic deposition in a low-waste process was proposed here as a possible alternative to the current technologies. The effect of the species involved in the single processes in the recirculated stream was evaluated, where a negligible influence of the sacrificial species (ethanol) in the leaching unit was noticed. Different home-prepared ZnO photocatalysts were tested, and the best performance in terms of recovery of palladium was obtained in the presence of ZnO nanoparticles prepared through sol–gel synthesis. The proposed procedure is a viable route for the recovery of Pd from spent catalysts: by combining the processes, the complete oxidation of palladium was observed in about 15 minutes, while the recovery of Pd through photodeposition on ZnO occurred within 120 minutes of irradiation.

1. Introduction

Nowadays, the depletion of resources and demographic growth, the increasing prices of raw materials, climate change and environmental problems related to production processes lead to recognition of the urgency to promote the development of a circular economy, through the study and the adoption of near-zero waste processes.[1–3] Metals are the best candidates to take a similar approach, being indefinitely recyclable, without any problem related to downcycling.[2,4,5] Among the recyclable materials, PGMs, and, in particular palladium, are the most interesting,[6,7] due to the great number of applications in which they are used,[7–14] such as catalytic converters, electronic devices and chemical production (see Fig. 1 for the percentage demand in different industrial applications). The European Union inserted platinum group metals in the list of 14 strategic materials, due to their key role in several industrial applications.[15] Looking specifically at palladium, it is certainly an expensive and relatively scarce element in the Earth's crust, with the mineral resources of PGMs predominately localized in South Africa and Russia.[16] A huge gap was recorded in the last few years between the growing demand for this material and its limited supply which

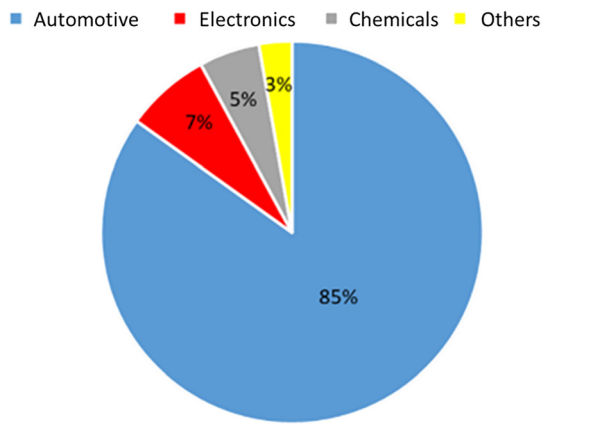

Fig. 1 Application demand for palladium in different industrial applications since 2016.[7]

[a] *Dipartimento di Ingegneria Chimica, dei Materiali e della Produzione Industriale, Università di Napoli "Federico II", Italy. E-mail: marica.muscetta@unina.it*
[b] *Department of Chemical Engineering, Center for Membranes and Advanced Water Technology (CMAT Center) and, Research and Innovation Center on CO_2 and Hydrogen (RICH Center), Khalifa University, P.O. Box 127788, Abu Dhabi, United Arab Emirates*
[c] *Istituto di Scienze e Tecnologie per l'Energia e la Mobilità Sostenibili (CNR), Napoli, Italy. E-mail: ilaria.disomma@stems.cnr.it*

† Electronic supplementary information (ESI) available. See DOI: https://doi.org/10.1039/d2re00240j

requires the development of appropriate strategies to be developed.[7] Recently, to overcome the shortage in palladium supply, several authors proposed and discussed the recycling of metals from end-of-life devices.[17–26]

At present, hydrometallurgical processes represent the most widely used approach for metal recovery,[27–32] despite the numerous operating units, the strong acidity and the high-temperature conditions required, and the polluting streams resulting from those treatments. In a previous study,[33] some of the authors proposed and discussed an alternative route for the dissolution of zero-valent palladium nanoparticles from solid wastes by means of NaCl and $CuCl_2$ under mildly acidic conditions, identifying the best chloride and cupric ion concentrations to optimize the leaching process.

Nowadays, leaching solutions containing dissolved palladium are generally treated by means of different processes such as precipitation, membrane separation and electrodeposition, for which low selectivities are recorded and numerous operating units are required.[22,34–39] An alternative was proposed by some of the authors in a recent study,[40] in which the recovery of palladium from the leaching solution was achieved through its photocatalytic deposition in the presence of ZnO under visible and UV-visible light irradiation.

Starting from a spent palladium catalyst, the effective recovery of the metal may be thus obtained from the adoption of two separate stages (leaching and photodeposition), although this approach leads to the generation of wastewater streams that need proper treatment before discharge into the environment (see below). In the following sections, a detailed description of a new process combining leaching and photodeposition stages is presented and discussed.

2. Combination of the leaching and photodeposition processes

In Fig. 2, the block diagrams of the processes for the palladium recovery are reported according to the results of previous studies.[33,40] The recovery of metallic palladium takes place from a spent catalyst in which the catalytic activity is based only on the presence of this metal. Referring to palladium, as reported previously and shown in Fig. 2(A), a solution containing NaCl/$CuCl_2$ (1) is used to oxidize Pd(0) to Pd(II), obtaining a waste not containing palladium species. The solution derived from the leaching unit (2) is successively treated, in the presence of ZnO nanoparticles in a photocatalytic reactor; in particular, as previously reported and shown in Fig. 2(B), the photodeposition process takes place in the presence of ethanol as a sacrificial agent, under UV-A/visible light irradiation. The resulting Pd/ZnO composite material is separated from the solution by filtration and washed, obtaining a waste solution containing NaCl, Cu^{1+} and

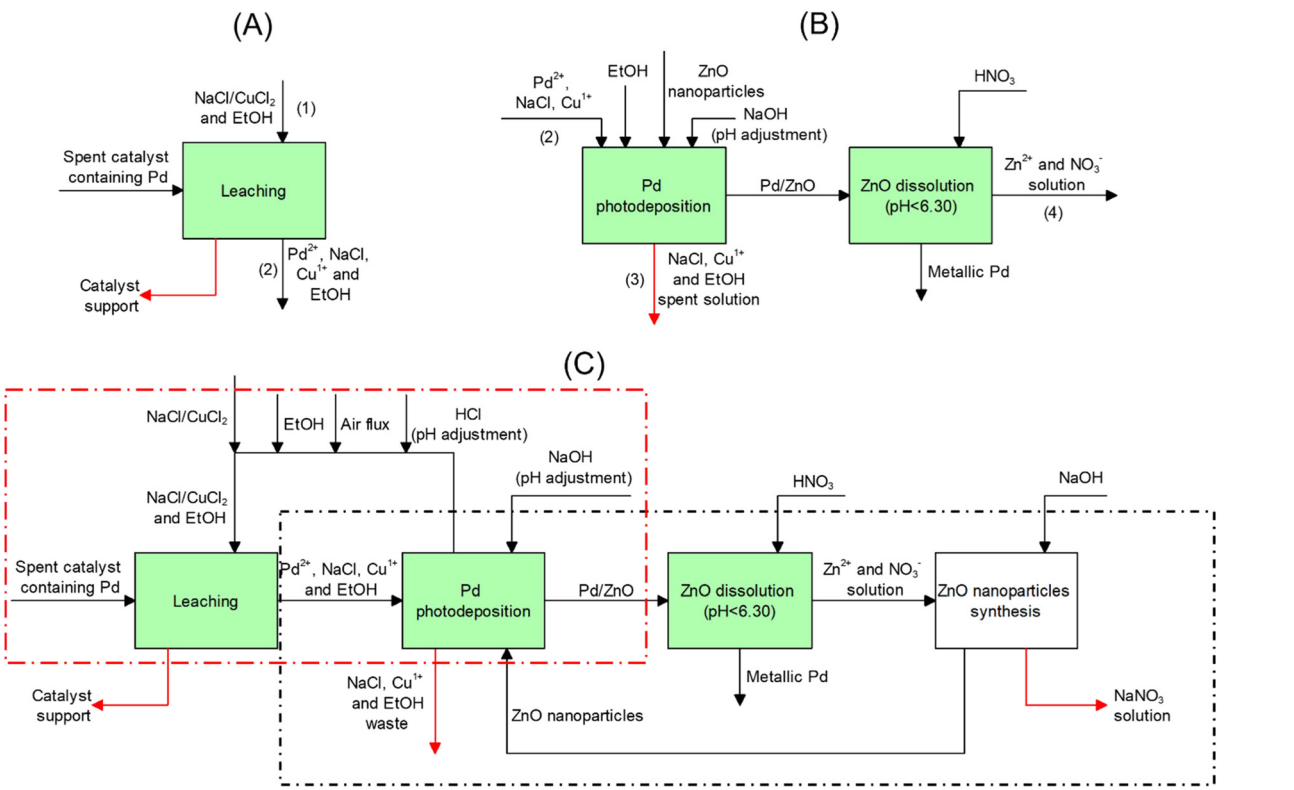

Fig. 2 Block diagram for the recovery of palladium from waste materials. (A) Leaching stage (the unit reported in green colour was studied in a previous study[33]), (B) photodeposition stage and recovery of metallic palladium (the units reported in green colour were analysed in a previous study[40]), (C) combined process with recycling (studied in the current work). Leaching and photodeposition units (red dashed box); photodeposition unit and preparation of the photocatalyst (black dashed box).

ethanol. As for the effective palladium recovery, the dissolution of zinc oxide nanoparticles, by adjusting the pH of the suspension below 6.30, was studied in a previous study.[41] Therefore, metallic palladium precipitates are recovered, while a stream containing zinc ions and nitrates is generated (4).

Table 1 shows the theoretical composition of the spent streams generated within the two processes, calculated according to the indications reported in previous papers[33,40] when the total recovery of palladium was achieved starting from a synthetic waste containing about 100 milligrams of the metal. It is evident from the scheme in Fig. 2(B) that the streams (3) and (4) have to be considered as waste for which a proper treatment has to be arranged to allow their disposal. However, as shown in the Table 1, despite the presence of ethanol, being stream (3) mainly composed of chloride and copper species, it could be possible to reuse it in a new leaching stage, thus reducing the produced wastes. Meanwhile, stream (4), coming from the dissolution of zinc oxide and containing zinc ions and nitrates, could be used to newly synthesize fresh zinc oxide particles to be recycled and used as a photocatalyst in the photodeposition stage.

According to the facts reported above, the present work evaluates the possibility of effectively recovering palladium from spent catalysts containing it, combining processes A and B (Fig. 2) in a single two-stage process (leaching + photodeposition) in which streams (3) and (4) are recycled from the outlet of the photoreactor to the leaching unit, focusing the attention on the influence of the recycled streams on the kinetics and yield of palladium recovery. In particular, the effect of ethanol (used as a sacrificial agent) on the leaching process is analysed, along with the need to re-oxidize the Cu(I) ions produced during the leaching stage and the makeup of these species required at the end of the sequence of the two stages to maintain a fixed recovery efficiency in the successive treatments. Finally, a procedure is developed for the preparation of ZnO photocatalyst particles from exhaust effluents – generated during the photodeposition stage – and tested as an effective way of recycling zinc in the overall process.

3. Materials and methods

3.1. Materials

Copper chloride ($CuCl_2$, powder, purity = 99%), sodium chloride (NaCl, purity ≥99%), zinc oxide (ZnO, nanopowder, <50 nm particle size (BET), purity >97% – used as a reference), palladium chloride ($PdCl_2$, purity = 99%), titanium dioxide nanopowder (TiO_2, commercial grade, Aeroxide P25, average particle size 21 nm, specific surface area 50 ± 15 $m^2\ g^{-1}$, 80/20 anatase/rutile), metallic palladium (Pd, powder, <1 μm, purity ≥99.9% – used as a reference), zinc acetate dihydrate (ZAD, purity ≥99.0%) and triethylamine (TEA, purity ≥99.0%) were purchased from Aldrich Chemistry. Ethanol (EtOH, purity ≥99.8%) was purchased from Fluka. Sodium hydroxide pellets (NaOH), hydrochloric acid (HCl, 37%), and nitric acid (HNO_3, 69%) were purchased from AnalaR BDH. Doubly glass-distilled water was used throughout this study.

Table 1 Theoretical compositions of the aqueous solutions coming from the blocks reported in Fig. 2

Species	(1)	(2)	(3)	(4)
Ethanol (M)	—	—	≈1.7	—
Cu^{2+} (mM)	2.5	—	—	—
Cu^{+} (mM)	—	2.5	2.5	—
Cl^{-} (M)	4.0	4.0	4.0	—
Na^{+} (M)	4.0	4.0	4.0	—
Zn^{2+} (mM)	—	—	—	30.0
NO_3^{-} (mM)	—	—	—	60.0
H_2O (l)	1	1	1	1

3.2. Experimental procedures

In the current work, ZnO nanoparticles were synthesized following different procedures:

3.2.1. Synthesis of ZnO nanoparticles *via* a sol–gel approach. Some photocatalytic materials were prepared through a sol–gel method, based on a recent article.[42] In particular, about 1 g of catalyst was obtained when 40.83 mL of 0.4 M NaOH was added dropwise to 61.25 mL of an aqueous solution of $Zn(NO_3)_2$ 0.2 M. After stirring at 500 rpm for 30 minutes, the solution was kept at room temperature for 18 hours to obtain a white gel. Afterwards, the gel was washed four times with distillate and dried at 80 °C in a fan-assisted oven (30%) for 24 hours. The obtained powder was calcined at fixed temperatures (200 °C and 500 °C) in air (ZnO–S air 200 °C and ZnO–S air 500 °C), and nitrogen (ZnO–S N_2 200 °C) for 2 hours, then it was tested and characterized.

3.2.2. Synthesis of ZnO nanoparticles *via* a solvothermal approach. ZnO nanoparticles (ZnO–H) were also prepared through a solvothermal approach, taking inspiration from our previously defined protocol.[43] First, a solution of the inorganic precursor was prepared by solubilizing 0.53 g of ZAD into an organic mixture of ethanol (144 mL) and TEA (3.36 mL). This solution was alternately stirred and sonicated for about 15 minutes to allow the complete dissolution of the acetate salt. Then, 16 mL of double-distilled water was added, thus resulting in a slight loss of transparency indicating that hydrolysis and condensation reactions started. The obtained mixture was inserted into a sealed Teflon mini-reactor, in which the liquid volume corresponded to 75% of the total one, which was placed in a circulating oven at 120 °C for 2 hours for the solvothermal treatment. The suspension of ZnO–H was collected by centrifugation at 12 500 rpm for 15 min and washed 3 times with double-distilled water.

3.2.3. Leaching and photodeposition procedures. Palladium leaching runs and photocatalytic palladium reduction were carried out based on the procedures reported in previous articles.[33,40] In particular, for all runs, a fixed amount of a spent catalyst (Pd/TiO_2) was added in a doubly distilled aqueous solution (C_{Pd/TiO_2} = 500 ppm; Pd^0 percentage = 21% wt) at pH = 5.0 and a temperature of 60 °C, containing fixed concentrations of $CuCl_2$ (2.5 mM), NaCl (6.0

M) and EtOH (1.71 M); when the leaching process was completed, the pH of the obtained solution was adjusted to 8.0, by adding sodium hydroxide, to prevent ZnO dissolution. Moreover, to prevent the reaction between the dissolved oxygen and photogenerated electrons, a nitrogen stream was bubbled into the solution starting 40 minutes before the beginning of the photocatalytic runs. ZnO nanopowder (500 ppm) was thus added to the mixture. During the photocatalytic experiments, performed at ambient temperature, nitrogen was continuously bubbled into the reactor, at a flow rate of 0.3 L min^{-1}. In all cases, to study the deposition of palladium, at fixed times, several liquid samples were collected. As for the recycling experimental runs, to oxidize the copper species used in the leaching process, an air stream was bubbled into the solution derived from the photodeposition unit, starting 30 minutes before the leaching process. The material obtained after the photodeposition process was recovered as described in a previous article.[40] After washing the Pd/ZnO photocatalyst several times, a stoichiometric amount of HNO_3 was added to an aqueous solution in which the solid was suspended, to convert ZnO to a $Zn(NO_3)_2$ solution and a metallic precipitate (zero-valent palladium). The prepared solution was used to re-prepare ZnO photocatalysts by using the above-described sol–gel method for successive photodeposition.

3.2.4. Analytical techniques and material characterization. The colorimetric determination of palladium was performed using a spectrophotometer Cary 100 UV-vis (Agilent technologies), as reported in a previous article,[33] while the total concentration of cupric and cuprous ions in solution was measured employing a colorimetric method using an analytical kit (Macherey-Nagel) based on oxalic acid bis-cyclohexylidene hydrazide (cuprizone), as reported previously,[44] finally, a colorimetric determination of Cu(I) was carried out according to Gahler.[45] The morphology of all the photocatalysts and the recovered materials was investigated through transmission electron microscopy (TEM), using an FEI Tecnai G2 200kV microscope (FEI, Hillsboro, OR, USA). The TEM sample was prepared by suspending the powder sample in 2-propanol, treating it with ultrasound, and finally depositing 3 μL of the suspension 2 consecutive times on a 300-mesh Cu grid provided by Tedpella. The solvent was then evaporated at room temperature. The nature of the crystalline phases in the nanostructures was determined through X-ray diffraction (XRD) analysis, using a Bruker D2 Phaser XRD with CuKα radiation, operating at diffraction angles 2θ ranging between 5 and 90° with a scan step-size of 0.05°. The optical properties of the photocatalysts were assessed by the results of Diffuse Reflectance Spectroscopy, in the wavelength range 220–800 nm, employing a SHIMADZU UV-2600 spectrophotometer. For this purpose, the powder-based catalysts were dispersed onto a $BaSO_4$ substrate (100% reflectance standard) and then analysed. The diffuse reflectance spectra of all the prepared photocatalysts were collected and converted to the corresponding absorption spectra through the Kubelka–Munk function. Direct band gap energies (E_g) were calculated as the intercept of the fitted line on the abscissa ($[F(R)hv]^2 = 0$), following the Tauc method, to detect any modifications in the optical properties caused by different synthesis strategies or calcination treatments. Scanning electron microscopy (SEM) was performed using a Nova NanoSEM to observe the morphology of samples. The SEM sample was prepared by placing a small amount of powder sample on carbon tape attached to a stainless-steel stub.

4. Results and discussion

Starting from the simplified schematics of processes A and B reported in Fig. 2 and moving towards a combining scheme (C in the same figure) some problems may be expected due to a different composition of the streams concerning those obtained when leaching and photodeposition were carried out as separate processes. In the following subsections, the effects of this difference in the composition of the streams will be analysed in detail.

4.1. Leaching process

Following the approach described above, it can be easily understood that the leaching stage requires evaluating (i) the effect of the presence of ethanol and (ii) the effect of the presence of cuprous ions (instead of cupric ones).

4.1.1. Effect of ethanol. According to Table 1, the stream (3) in scheme B of Fig. 2 contains chlorides and cuprous ions (that could be easily converted into cupric ions) – at concentrations near those reported as optimal to dissolve palladium in a previous paper (6 M and 2.5 mM, respectively) – for which it was proposed to recirculate it to the leaching unit. Table 1 indicates the presence in this stream also of ethanol, whose effects on the leaching stage were not reported in the literature. Therefore, it was considered necessary to investigate the effect of ethanol on the metal dissolution process. For this purpose, a comparison between the results, in terms of palladium oxidation yield against time ($X_{Pd} = [Pd^{2+}]/[Pd^0]_{t=0}$), in the presence and absence of ethanol, is reported in Fig. 3. The figure highlights that the presence of ethanol (1.71 M) does not influence the leaching process, probably because it does not react with the present species.

4.1.2. Effect of airflow and Cu(I)–Cl makeup on the leaching process. Along with ethanol, the solution derived from the photocatalytic process contains, as reported in the previous section, sodium chloride and copper ions (Cu(I) and/or Cu(II)). In the previous work,[40] as indicated in reaction (r.1), the oxidation of metallic palladium in the leaching process requires the reduction of copper(II) to copper (I), as clearly shown in Fig. 4(a). For this reason, to recirculate the stream coming from the photodeposition stage to the leaching one, it is necessary to provide an air stream bubbling in the solution to completely re-oxidize copper(I) to copper(II), the latter representing the active species for the leaching of metallic palladium (r.1).

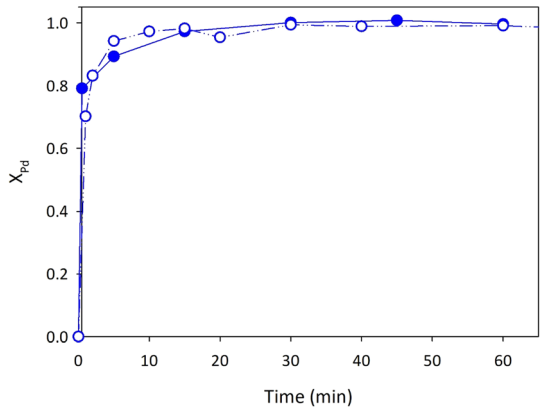

Fig. 3 Leaching step: evolution of the dissolved palladium fraction in aqueous solution in the presence (full symbols) and absence (empty symbols) of ethanol. Experimental conditions: pH = 5.0; $C_{Pd(0)}$ = 106 mg L^{-1}; $[Cu^{2+}]_0/[Pd^0]_0$ = 2.5; V = 0.2 L; T = 60 °C; $[NaCl]_0$ = 6.0 (M); [ethanol] (if present) = 1.71 M.

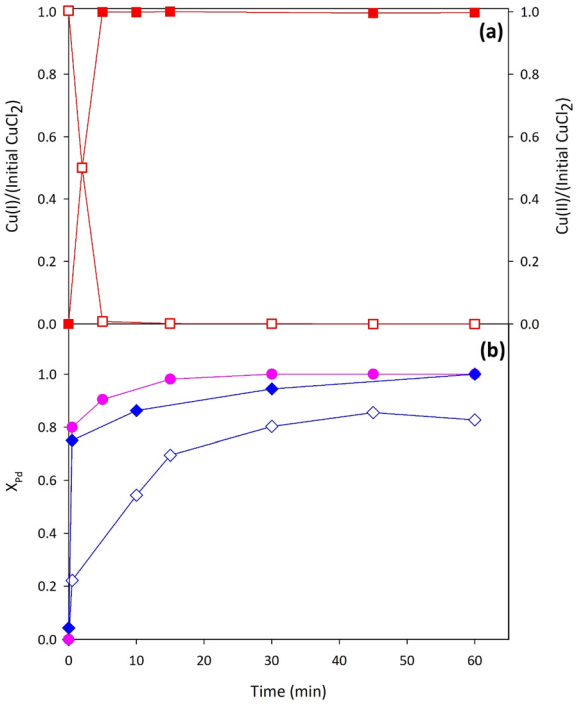

Fig. 4 (a) Copper(I) (■) and copper(II) (□) evolution during a typical leaching process; (b) palladium(II) evolution in a typical leaching run (●), with a recycled solution with (♦) and without air stream (◊). Experimental conditions: $C_{Pd(0)}$ = 106 mg L^{-1}; $[CuCl_2]/[Pd(0)]_0$ = 2.5; [NaCl] = 6.0 M; [EtOH] = 1.71 M; T = 60 °C; pH = 5.0; V = 0.2 L.

$$\frac{1}{2}Pd^0 + Cu^{2+} + 4Cl^- \rightleftarrows \frac{1}{2}PdCl_4^{2-} + CuCl_2^- \qquad (r.1)$$

Fig. 4(b) shows a comparison (in terms of palladium yield oxidation (X_{Pd}) *vs.* time) between the results obtained in a typical leaching process concerning those obtained with a recycled solution, previously submitted to an air stream bubbling (full symbols) or not (empty symbols). In the latter case, a slower palladium oxidation occurs, with a maximum conversion of about 80%. This result can be probably ascribed to the oxidation of a certain amount of copper(I) (formed during the first leaching stage) by the oxygen dissolved in the solution during the recycling. In contrast, the results obtained in the presence of the recycled solution – in which an air stream was bubbled starting 30 minutes before the leaching run – are comparable to those obtained using fresh leaching solutions, thus confirming the effectiveness of the recycling process.

Moreover, an evaluation of the total copper and chloride amounts eventually lost during the separation and the washing of the solid phase from the suspension (about 15% with respect to the feed) allowed establishment of the suitable makeup of these species at the leaching unit.

4.2. Photodeposition process

In the previous paper,[40] the recovery of palladium coming from the leaching solution through a photodeposition process was proposed, focusing attention on the effect of the radiation intensity, the sacrificial agent concentration, and the catalyst load. Moreover, considering the properties of ZnO to dissolve at certain pH values, an assessment of the best choice of the suspension pH was performed. In the next subsections, the influence of some operative variables on the photodeposition stage has been investigated, focusing on the possibility to recover the solutions as well as the photocatalytic material used.

4.2.1. Effect of ethanol make-up on the photodeposition process. As discussed in section 4.1.1, the solution derived from the photodeposition stage, containing the leaching reagents and ethanol, may be recirculated to the leaching unit. To maintain a constant photocatalytic efficiency, in terms of the deposition degree of palladium with time, it is necessary to evaluate the makeup of the sacrificial agent required before the recycling of the solution. As demonstrated previously, the presence of ethanol in the solution does not influence the leaching process, while a different behaviour of the photocatalytic system was previously observed by varying its concentration.[40] In Fig. 5, the efficiency of the photocatalytic Pd(II) reduction during a typical photocatalytic experiment, in the presence of commercial ZnO, was reported for (i) a run with a fresh solution, (ii) a run with a recirculated solution in which no fresh ethanol was added, and (iii) a run with a recirculated solution in which an amount of ethanol was added to the solution to reach a concentration similar to that adopted in the previous work on photodeposition. For this purpose, the loss of ethanol due to stripping by air stream bubbling to re-oxidize cuprous species, and the consumption during palladium deposition was calculated. As clearly shown by the diagram, the recovery efficiency was not significantly modified by varying the make-up of ethanol, probably due to the high concentration of the sacrificial species present in the solution used in the photocatalytic process.

4.2.2. Effect of different home-prepared ZnO photocatalysts. As indicated in the previous section, the

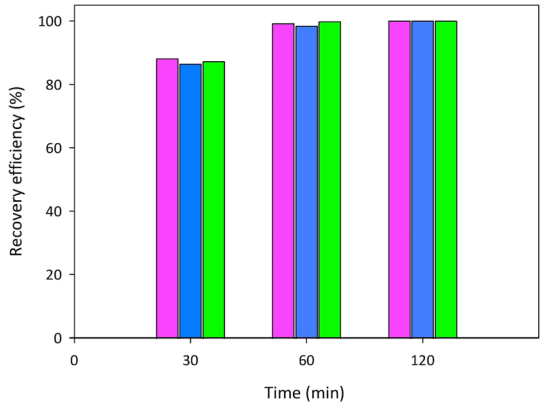

Fig. 5 Metal recovery efficiency (zero-valent palladium) with time during different photocatalytic runs: (■) photocatalytic run) (■) photocatalytic run with the recycled solution, with make-up of ethanol; (■) photocatalytic run with the recycled solution, without make-up of ethanol. Experimental conditions: C_{ZnO} = 500 ppm (commercial ZnO); $[Pd(II)]_0$ = 1.0 mM; [Cu(I)] = 2.5 mM; [NaCl] = 6.0 M; [EtOH] = 1.71 M; T = 25 °C; pH = 8.0; V = 0.2 L.

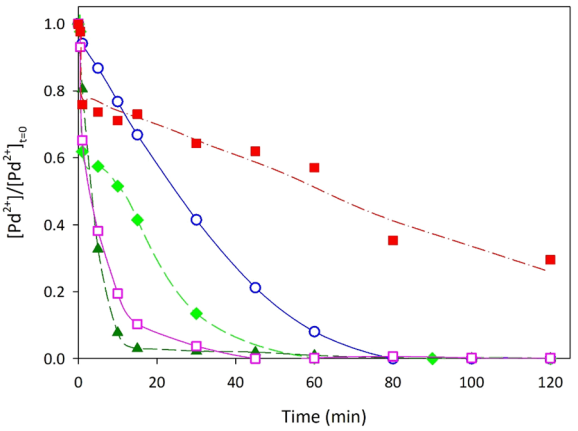

Fig. 6 Palladium(II) evolution during photocatalytic runs in the presence of different home-prepared zinc oxide photocatalysts. Experimental conditions: C_{ZnO} = 500 ppm; $[Pd(II)]_0$ = 1.0 mM; [Cu(I)] = 2.5 mM; [NaCl] = 6.0 M; [EtOH] = 1.71 M; T = 25 °C; pH = 8.0; V = 0.2 L. (■) ZnO–S N_2 200 °C; (□) ZnO–S air 500 °C; (▲) ZnO–S air 200 °C; (○) ZnO–H; (♦) commercial ZnO as a reference.

stream (4), coming from the dissolution of zinc oxide, is mainly composed of zinc ions and nitrates (when nitric acid is used to dissolve the ZnO photocatalyst). In the present research, the possibility to reuse the solution containing zinc ions to newly prepare zinc oxide semiconductors is proposed. For this purpose, the effect of different home-prepared zinc oxide photocatalysts was evaluated for palladium(II) photoreduction. As reported in the experimental section, four different types of zinc oxide samples were prepared, by adopting (1) a sol–gel method, followed by calcination under air or a nitrogen atmosphere at selected temperatures, and (2) a solvothermal method, based on a previous protocol.[43]

The behaviour of the different materials was analysed, focusing on (i) the photocatalytic activity and (ii) the preparation methods.

In Fig. 6, the palladium evolution *versus* reaction time was reported in the presence of different zinc oxide photocatalysts. As clearly shown by the trend lines, the highest photocatalytic reactivity was recorded in the presence of air calcined photocatalysts. All the materials prepared through the sol–gel method highlighted a trend typical for such processes, indicating an adsorption phenomenon at the initial stage of the photodeposition, as reported also for the benchmark photocatalyst (commercial ZnO). Moreover, the increase of the calcination temperature from 200 °C to 500 °C appears to have only a small influence on the photocatalytic deposition of palladium. As for the ZnO photocatalyst prepared through hydrothermal synthesis, a lower activity was recorded, despite a complete photoreduction observed after 80 minutes of irradiation. The lower reactivity can be probably ascribed to the different morphology of the material, for which initial adsorption was not observed.

It is clear that, in the latter case, the dissolution of zinc oxide – proposed in section 2 to recover the metallic Pd by adjusting the pH of the suspension below 6.30 – should be performed with acetic acid, thus obtaining a fresh precursor for the hydrothermal synthesis. This alternative preparation method was herein proposed because, from an environmental point of view, the use of organic acids might be preferred to that of nitric acid. Nevertheless, based on the above-reported considerations on the photocatalytic activity, the material prepared through the sol–gel method and calcination in air at a temperature of 200 °C was chosen as a photocatalyst for further deposition of palladium.

4.3. Materials characterization

In this subsection, a thorough characterization of the best photocatalyst tested (ZnO–S air 200 °C) will be analysed and discussed, along with the recovered Pd/ZnO composite, the recovered metal, and the newly prepared and recycled photocatalysts. As a comparison, the characterization of the ZnO nanoparticles prepared through the solvothermal approach (ZnO–H) will be investigated.

Estimated E_g values are collected in Table S1.† Fig. 7 shows the $[F(R)hv]^2$ function against photon energy for all the fresh photocatalysts. Tauc-plot linearization (inset in Fig. 7) points out that the 3.23 eV band gap is estimated for ZnO–S air 200 °C and a very similar value was obtained for ZnO–H, confirming the value found by Vitiello *et al.*[43] for ZnO nanoparticles produced through a similar hydrothermal route. This E_g is associated with the direct transition between the O_{2p}–Zn_{3d} valence band and the Zn_{4s}–Zn_{4p} conduction band.[46,47] A minor enhancement of the band gap is detected when calcination is carried out at a higher temperature (ZnO–S air 500 °C) or under a N_2 flux (ZnO–S N_2 200 °C). Similarly, E_g rises for photocatalysts obtained through single (ZnO–S air 200 °C-II) and double (ZnO–S air 200 °C-III) recycling of stream (4) with respect to freshly prepared ZnO–S air 200 °C

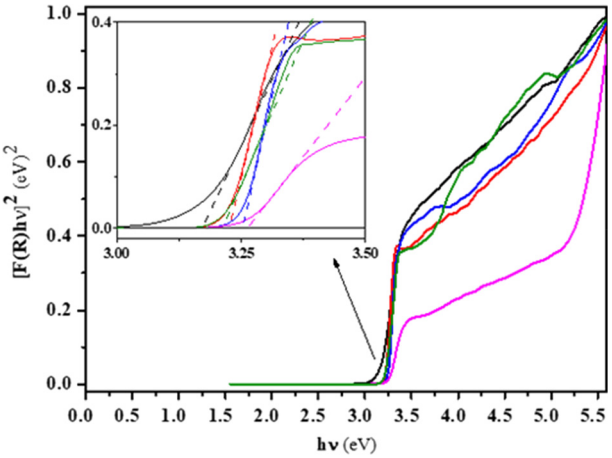

Fig. 7 Tauc-plot linearization of DRUV-vis spectra for commercial ZnO (black), ZnO–S air 200 °C (red), ZnO–S air 500 °C (blue), ZnO–S N_2 200 °C (magenta), and ZnO–H (olive). Inset at the top left indicates the 3.0–3.5 eV region with the linear extrapolations for each curve (dashed lines).

(Fig. 8). As for commercial ZnO, it exhibits the lowest band gap, equal to 3.18 eV and significantly narrower than those reported in the literature.[48–50] This could be due to the important Al doping (6%) of the reference materials used, which cause defects in the wurtzite lattice with the consequent shrinking of the band gap for Al doping higher than 1.5%.[51]

In Fig. 9, XRD diffraction patterns are reported for different materials (commercial ZnO and commercial Pd), ZnO prepared through the sol–gel method (ZnO–S air 200 °C), ZnO newly prepared after one (ZnO–S air 200 °C I) and two dissolutions (ZnO–S air 200 °C II), the Pd/ZnO composite material (Pd/ZnO (S air 200 °C)) and the recovered Pd. The peaks in all ZnO spectra can be indexed to the hexagonal phase of ZnO (wurtzite) and the face-centered cubic phase for

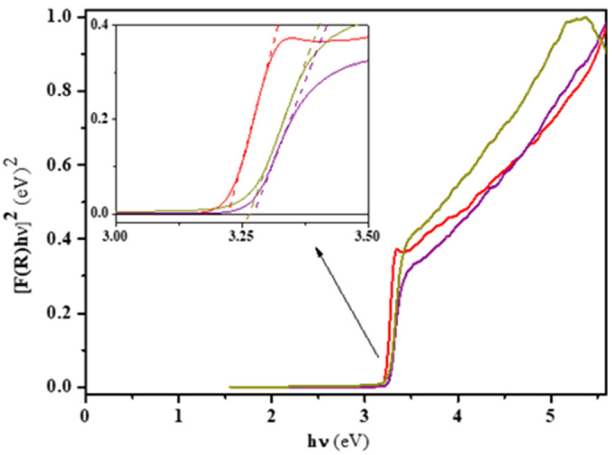

Fig. 8 Tauc-plot linearization of DRUV-vis spectra for ZnO–S air 200 °C (red), ZnO–S air 200 °C – II (purple), and ZnO–S air 200 °C – III (dark yellow). Inset at the top left indicates the 3.0–3.5 eV region with the linear extrapolations for each curve (dashed lines).

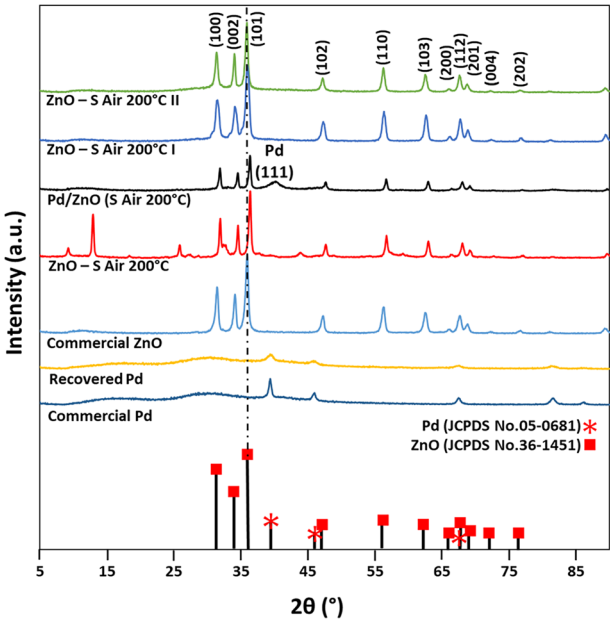

Fig. 9 XRD patterns of the tested materials.

Pd. The ZnO and Pd peaks agreed well with the reported literature diffraction peak values for ZnO (JCPDS no. 36-1451) and Pd (JCPDS no. 05-0681). In the case of the sol–gel synthesized ZnO, additional peaks were observed, indicating the likely presence of impurities, while the shifting in the diffraction peaks of the ZnO sample is typical for the home-prepared materials. The presence of metallic palladium was confirmed by the Pd/ZnO spectra, in which a peak corresponding to Pd(111) was observed. The crystallite size and the crystallinity of the sol–gel synthesized ZnO are larger than that of the commercial sample. The crystallite size and the crystallinity of the recovered Pd are smaller than that of the commercial sample. Hydrothermal synthesis conditions did not result in any changes in the diffraction pattern of ZnO–H if compared to the other presented photocatalysts (Fig. S1†), confirming the formation of a proper wurtzite lattice (JCPDS no. 36-1451).

The comparison between the SEM images of the commercial ZnO and that prepared through sol–gel synthesis, reported in Fig. 10, demonstrated a smaller size of agglomerates (*ca.* 100 nm), mostly spherical-like in shape in the first case, while the home-prepared samples show a larger size of agglomerates (*ca.* 500 nm), with shapes varying from spherical-like to plate-like to rod-like. The newly prepared samples (ZnO–S air 200 °C I and II) show more agglomerates than the fresh sample (ZnO–S air 200 °C), mostly spherical-like and plate-like in shape (see Fig. S2†). As concerns the Pd/ZnO sample, recovered after the photocatalytic deposition of palladium (see Fig. S3†), the size of the agglomerates (*ca.* 50 nm) is much smaller than that of the ZnO sample (ZnO–S air 200 °C), with a morphology more homogeneous than that of ZnO–S air 200 °C and most particle agglomerates are spherical-like in shape.

Moreover, in Fig. 11, the TEM micrographs of the recovered palladium are reported. As clearly shown by the

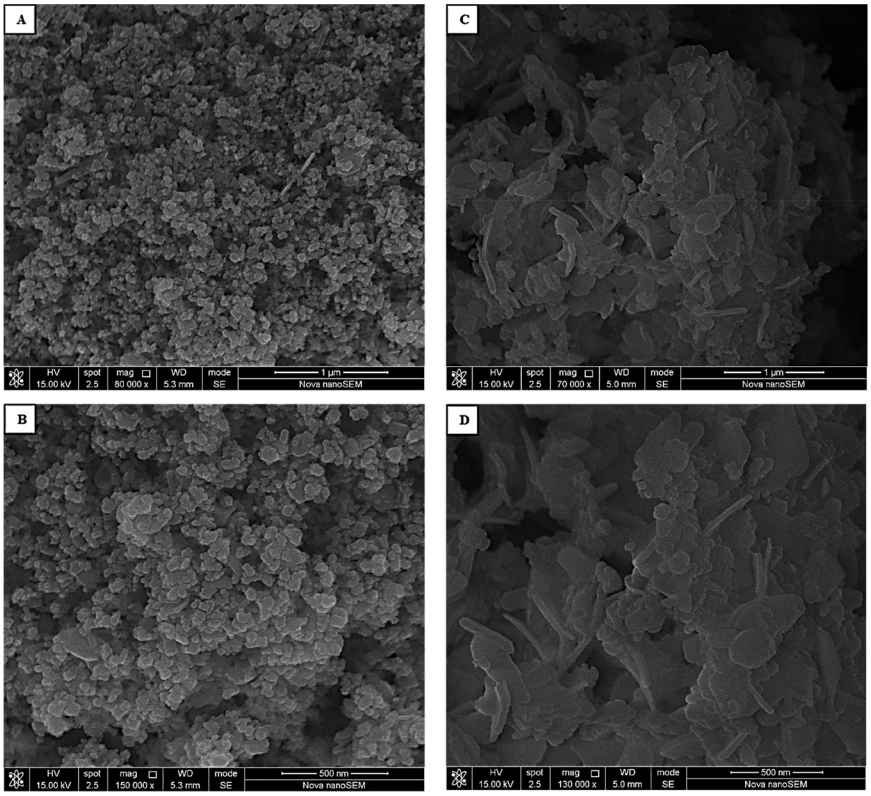

Fig. 10 SEM images of commercial ZnO (A and B) and ZnO samples (ZnO–S air 200 °C (C and D)) prepared through sol–gel synthesis.

figure, the recovered metal shows particle sizes ranging from 2 to 5 nm (see Fig. S4†).

Concerning the morphology of the ZnO samples, micrographs for the ZnO–H sample (Fig. 12A and B) display the presence of rod-like nanostructures with a diameter of about 10 nm and a heterogeneous length distribution ranging from 10 to 150 nm (see Fig. S5†). An alkaline pH allows for the enlargement of ZnO particles due to the migration of ZnO_2^{2-} anions from the hydro-alcoholic reaction mixture to primary ZnO nuclei. Moreover, the anisotropic shape of rods is attributed to the presence of TEA, which acts as a chelating agent for Zn^{2+} cations, preventing ZnO nanostructures from radial expansion.[52] Furthermore, micrographs of ZnO–S air 200 °C (Fig. 12C and D) show the presence of shapes varying from spherical-like to hexagonal-like to rod-like, with a larger size of particles (50–500 nm). The different morphology observed for ZnO–H and ZnO–S air 200 °C may be related to the different reactivity recorded in the presence of the two different photocatalysts, as reported in the previous section (see Fig. 6). Finally, the comparison of the TEM micrographs of the fresh ZnO (Fig. 12C and D) to the newly prepared samples (Fig. 12E–H, obtained through sol–gel synthesis) shows that the morphology of sol–gel ZnO particles did not change after being recycled, while the size of particles seems to decrease after every regeneration cycle.

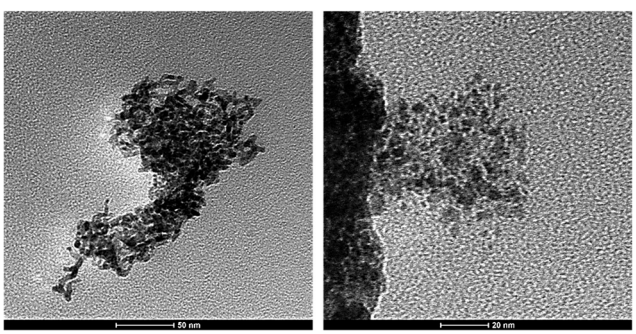

Fig. 11 TEM images of palladium recovered through photodeposition.

4.4. Photocatalyst recycling

The chosen material was used to evaluate the possibility of effectively reusing the solution containing zinc ions and nitrates for the newly prepared photocatalyst. As clearly shown in Fig. 13, the photocatalytic activity in the presence of the newly prepared materials is comparable to that obtained with the fresh sample, thus indicating the possibility to recycle the stream (4). The comparison between the XRD patterns of the fresh samples and the samples prepared from zinc recovery (see Fig. 8) indicates a similar crystalline structure of the three materials, thus confirming the effectiveness of this choice, despite some impurities being observed in the fresh sample, which are probably not fully eliminated during the washing procedure. The moderate reduction in the photodeposition rate may be ascribed to the higher agglomeration of the particles of the newly prepared

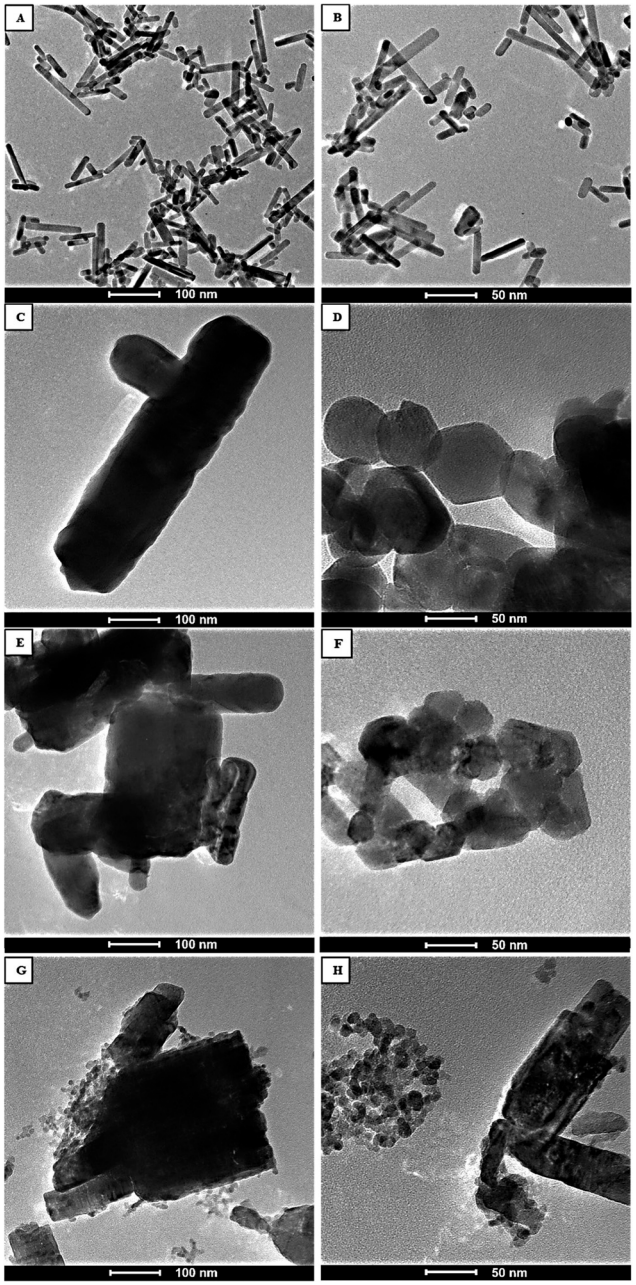

Fig. 12 (A and B): TEM images of ZnO–H nanorods taken at lower (A) and higher magnification (B); (C and D): TEM images of ZnO–S air 200 °C taken at lower (C) and higher magnification (D); (E and F): TEM images of ZnO–S air 200 °C I, taken at lower (E) and higher magnification (F and H): TEM images of ZnO–S air 200 °C II, taken at lower (G) and higher magnification (H).

samples with respect to the fresh material, as clearly indicated in the SEM images reported in Fig. 9 and previously discussed.

4.5. Reuse of the leaching solution

To conclude this investigation on the possibility to combine the leaching and photocatalytic deposition processes of palladium, some experimental runs were performed with

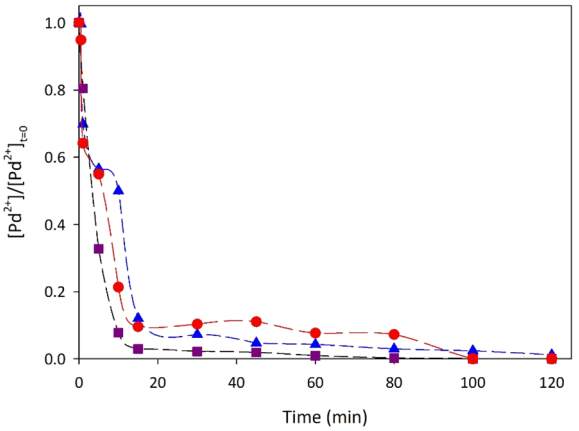

Fig. 13 Palladium(II) evolution in the presence of the ZnO photocatalyst prepared through calcination in air at 200 °C for 2 hours (ZnO–S air 200 °C), during photocatalytic runs in which zinc oxide was dissolved and prepared three times: (■) first photocatalytic run, (●) second photocatalytic run, and (▲) third photocatalytic run. Experimental conditions: C_{ZnO} = 500 ppm; $[Pd(II)]_0$ = 1.0 mM; [Cu(I)] = 2.5 mM; [NaCl] = 6.0 M; [EtOH] = 1.71 M; T = 25 °C; pH = 8.0; V = 0.2 L.

more than one recycling of the solution coming from the photocatalytic unit. Starting from a spent Pd^0/TiO_2 catalyst, the leaching stage was carried out; then, the best-tested photocatalyst was used for the photodeposition (ZnO–S air 200 °C). Once the material Pd/ZnO has been separated, the solution from the photodeposition process has been treated with airflow, as the presence of cuprous ions requires the oxidation of copper(I) to copper(II), the latter being the active species in the leaching process. A second (and third) aliquot of the spent Pd^0/TiO_2 catalyst was thus used to carry out the successive leaching and photodeposition stages. In Fig. 14 the results (in terms of Pd^{2+} evolution *vs.* time, with respect to the initial Pd^0) in the single "two-stage process" were reported. As indicated in the diagrams, regarding the leaching process, the effectiveness to recirculate the solution coming from the photodeposition stage was confirmed, obtaining the complete oxidation of palladium in about 15 minutes; moreover, in all photocatalytic stages, the photodeposition of palladium occurred within 120 minutes of irradiation.

5. Proposed mechanism

Fig. 15 shows the schematic illustration of the mechanism of the main stages of the proposed process. In the first block, the leaching of palladium occurs through the reaction (r.1); as previously discussed,[33] the volume of the zero-valent palladium particles progressively decreases with time, as a result of the leaching reaction taking place at the palladium/solution interface. Then, the palladium ions, obtained from the leaching stage, can react under UV-visible light irradiation in the presence of ZnO nanoparticles (prepared through sol–gel synthesis): in particular, as discussed in a previous article[40] and reported in Fig. 15, palladium ions can be reduced to metallic Pd through the reaction with the

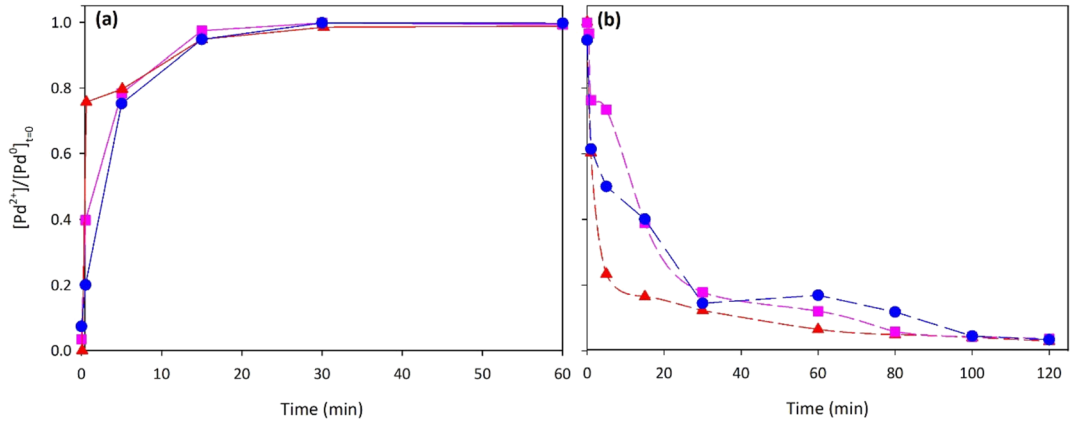

Fig. 14 Evolution of palladium(II) with time during the three "two-stage processes (leaching + photodeposition)". (▲) First stage, (●) second stage, and (■) third stage. Experimental conditions: (a) leaching stage: $C_{Pd(0)}$ = 106 mg L^{-1} (starting from spent Pd^0/TiO_2 catalyst); $[CuCl_2]/[Pd(0)]_0$ = 2.5; [NaCl] = 6.0 M; [EtOH] = 1.71 M; T = 60 °C; pH = 5.0; V = 0.2 L. (b) Photodeposition stage: C_{ZnO} = 500 ppm (ZnO–S air 200 °C); T = 25 °C; pH = 8.0; V = 0.2 L.

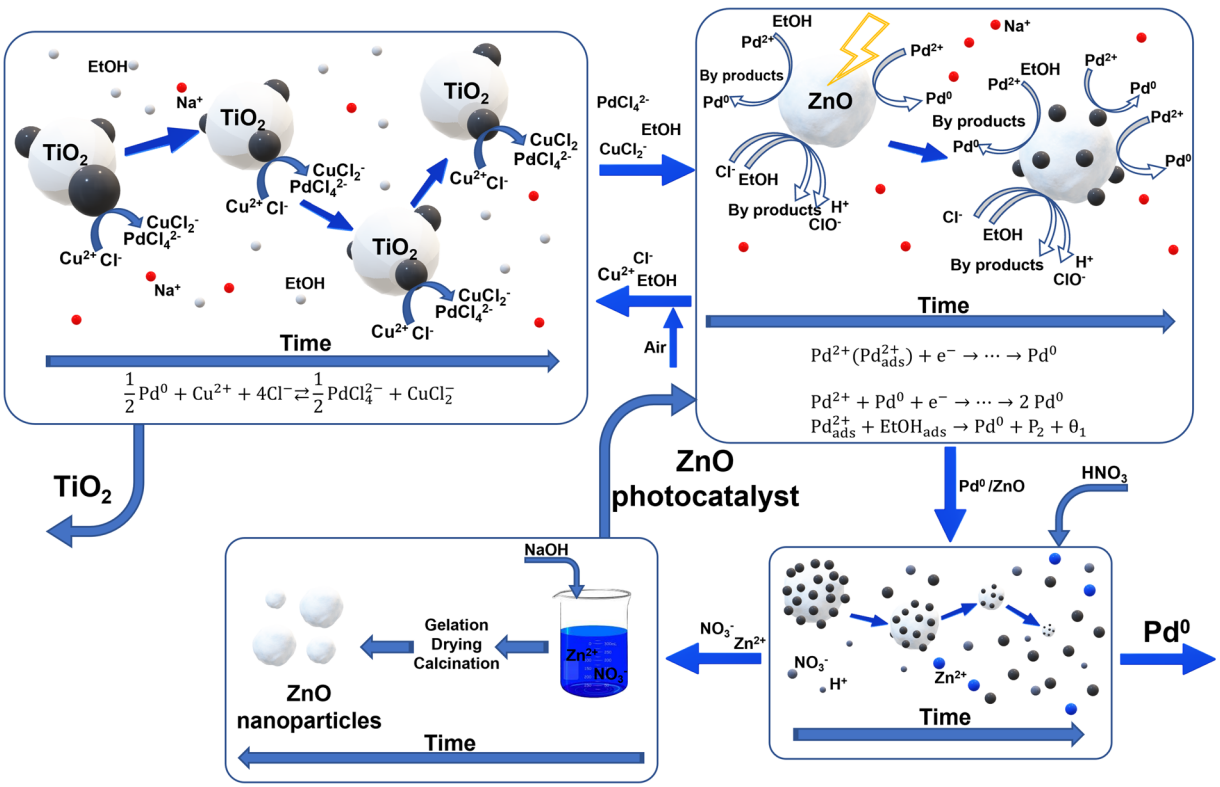

Fig. 15 Schematic representation of the reaction mechanisms for the main stages of the process.

photogenerated electrons. Moreover, the formation of the metal catalyzes further palladium reduction. Finally, ethanol adsorbed on the catalyst surface may react with the adsorbed palladium, producing again metallic Pd and by-products.

Conclusions

The recovery of palladium from spent catalysts containing palladium by combining leaching and photodeposition processes was investigated, focusing attention on the influence of the recycled streams on the kinetics and yield of palladium recovery. In particular, the presence of ethanol in the recirculated stream seems to not influence the leaching process, possibly because it does not react with the present species, and the recovery efficiency was not modified after varying the make-up of ethanol, probably due to the high concentration of the sacrificial species in a single photocatalytic step. Different home-prepared ZnO

photocatalysts were synthesized and tested, focusing on (i) the photocatalytic activity and (ii) the preparation methods. Based on the results obtained, ZnO nanoparticles prepared through sol–gel synthesis, calcined at 200 °C, are suggested to be suitable for the recovery of palladium. The proposed procedure for the preparation of ZnO photocatalyst particles may be considered as an effective way of recycling zinc within the overall process. The effective combination of the leaching and photocatalytic deposition processes was confirmed, obtaining the complete oxidation of palladium after 15 minutes and the total photocatalytic deposition of palladium within 120 minutes of irradiation. Despite a mere comparison between the proposed process and those reported in the literature being difficult, the use of mild acidic conditions and the possibility to effectively reuse the solution containing zinc ions and nitrates to newly prepare photocatalyst make the process potentially attractive in the metal recovery field.

Conflicts of interest

There are no conflicts to declare.

References

1 J. Spooren, K. Binnemans, J. Björkmalm, K. Breemersch, Y. Dams, K. Folens, M. González-Moya, L. Horckmans, K. Komnitsas, W. Kurylak, M. Lopez, J. Mäkinen, S. Onisei, K. Oorts, A. Peys, G. Pietek, Y. Pontikes, R. Snellings, M. Tripiana, J. Varia, K. Willquist, L. Yurramendi and P. Kinnunen, *Resour., Conserv. Recycl.*, 2020, **160**, 104919.
2 D. Giurco, A. Littleboy, T. Boyle, J. Fyfe and S. White, *Resources*, 2014, **3**, 432–453.
3 Y. Kalmykova, M. Sadagopan and L. Rosado, *Resour., Conserv. Recycl.*, 2018, **135**, 190–201.
4 C. Hagelüken, J. U. Lee-Shin, A. Carpentier and C. Heron, *Recycling*, 2016, **1**, 242–253.
5 M. Jackson, A. Lederwasch and D. Giurco, *Resources*, 2014, **3**, 516–543.
6 D. I. Kim, G. Gwak, P. Dorji, D. He, S. Phuntsho, S. Hong and H. Shon, *ACS Sustainable Chem. Eng.*, 2018, **6**(2), 1692–1701.
7 J. Matthey, *PGM market report May 2021*, 2021, pp. 1–48.
8 C. Saguru, S. Ndlovu and D. Moropeng, *Hydrometallurgy*, 2018, **182**, 44–56.
9 Y. Lu and Z. Xu, *Resour., Conserv. Recycl.*, 2016, **113**, 28–39.
10 I. Saldan, Y. Semenyuk, I. Marchuk and O. Reshetnyak, *J. Mater. Sci.*, 2015, **50**, 2337–2354.
11 Y. Li, C. Zhang, J. Ma, M. Chen, H. Deng and H. He, *Appl. Catal., B*, 2017, **217**, 560–569.
12 O. F. Aldosari, S. Iqbal, P. J. Miedziak, G. L. Brett, D. R. Jones, X. Liu, J. K. Edwards, D. J. Morgan, D. K. Knight and G. J. Hutchings, *Catal. Sci. Technol.*, 2016, **6**, 234–242.
13 W. Liang, X. Du, Y. Zhu, S. Ren and J. Li, *Catalysts*, 2020, **10**(3), 347.
14 B. Tapin, F. Epron, C. Especel, B. K. Ly, C. Pinel and M. Besson, *ACS Catal.*, 2013, **3**, 2327–2335.
15 N. Florin, B. Madden, S. Sharpe, S. Benn, R. Agarwal, R. Perey and D. Giurco, *Shifting Business Models for a Circular Economy: Metals Management for Multi-Product-Use Cycles*, 2015, vol. 10.
16 Y. K. Taninouchi and T. H. Okabe, *Metall. Mater. Trans. B*, 2018, **49**, 1781–1793.
17 M. H. Morcali, *Resour., Conserv. Recycl.*, 2020, **159**, 104891.
18 H. Li, J. Eksteen and E. Oraby, *Resour., Conserv. Recycl.*, 2018, **139**, 122–139.
19 C. H. Kim, S. I. Woo and S. H. Jeon, *Ind. Eng. Chem. Res.*, 2000, **39**, 1185–1192.
20 D. Xun, H. Hao, X. Sun, Z. Liu and F. Zhao, *J. Cleaner Prod.*, 2020, **266**, 121942.
21 Y. Ding, S. Zhang, B. Liu, H. Zheng, C. C. Chang and C. Ekberg, *Resour., Conserv. Recycl.*, 2019, **141**, 284–298.
22 A. M. Yousif, *J. Chem.*, 2019, 1–7.
23 D. Bourgeois, V. Lacanau, R. Mastretta, C. Contino-Pépin and D. Meyer, *Hydrometallurgy*, 2020, **191**, 105241.
24 V. T. Nguyen, S. Riaño, E. Aktan, C. Deferm, J. Fransaer and K. Binnemans, *ACS Sustainable Chem. Eng.*, 2021, **9**, 337–350.
25 Y. Chen, M. Xu, J. Wen, Y. Wan, Q. Zhao, X. Cao, Y. Ding, Z. L. Wang, H. Li and Z. Bian, *Nat. Sustain.*, 2021, **4**, 618–626.
26 S. E. Can Sener, V. M. Thomas, D. E. Hogan, R. M. Maier, M. Carbajales-Dale, M. D. Barton, T. Karanfil, J. C. Crittenden and G. L. Amy, *ACS Sustainable Chem. Eng.*, 2021, **9**, 11616–11634.
27 D. Fontana, M. Pietrantonio, S. Pucciarmati, G. Nadia and T. Chiara, *J. Mater. Cycles Waste Manage.*, 2018, **20**, 1199–1206.
28 Y. Ding, H. Zheng, B. Liu and C. Ekberg, *Materials*, 2019, **12**(8), 1205.
29 C. A. Nogueira, A. P. Paiva, M. C. Costa and A. M. R. da Costa, *Environ. Technol.*, 2019, 1–11.
30 M. K. Jha, J. C. Lee, M. S. Kim, J. Jeong, B. S. Kim and V. Kumar, *Hydrometallurgy*, 2013, **133**, 23–32.
31 M. A. Barakat, G. A. EL-Mahdy, M. Hegazy and F. Zahran, *Open Miner. Process. J.*, 2009, **2**, 31–36.
32 U. Jadhav and H. Hocheng, *Sci. Rep.*, 2015, **5**, 1–10.
33 M. Muscetta, N. Minichino, R. Marotta, R. Andreozzi and I. Di, *J. Hazard. Mater.*, 2021, **404**, 124184.
34 A. Behnamfard, M. M. Salarirad and F. Veglio, *Waste Manage.*, 2013, **33**, 2354–2363.
35 D. Bourgeois, V. Lacanau, R. Mastretta, C. Contino-Pépin and D. Meyer, *Hydrometallurgy*, 2020, **191**, 105241.
36 J. Y. Lee, B. Raju, B. N. Kumar, J. R. Kumar, H. K. Park and B. R. Reddy, *Sep. Purif. Technol.*, 2010, **73**, 213–218.
37 Ş. Sarioğlan, *Platinum Met. Rev.*, 2013, **57**, 289–296.
38 Z. Zhang and F. S. Zhang, *J. Hazard. Mater.*, 2014, **279**, 46–51.
39 Y. Chen, Q. Qiao, J. Cao, H. Li and Z. Bian, *Joule*, 2021, **5**, 3097–3115.
40 M. Muscetta, R. Andreozzi, R. Marotta and I. di Somma, *J. Environ. Chem. Eng.*, 2021, **9**, 106523.
41 M. Muscetta, R. Andreozzi, R. Marotta and I. di Somma, *J. Environ. Chem. Eng.*, 2021, **9**, 106523.

42 A. Sangeetha, S. Jaya Seeli, K. P. Bhuvana, M. A. Kader and S. K. Nayak, *J. Sol-Gel Sci. Technol.*, 2019, **91**, 261–272.
43 G. Vitiello, G. Iervolino, C. Imparato, I. Rea, F. Borbone, L. de Stefano, A. Aronne and V. Vaiano, *Sci. Total Environ.*, 2021, **762**, 143066.
44 M. Muscetta, L. Clarizia, C. Garlisi, G. Palmisano, R. Marotta, R. Andreozzi, F. Ii, I. Chimica and P. Industriale, *Int. J. Hydrogen Energy*, 2020, **51**, 26701–26715.
45 A. R. Gahler, *Bunseki Kagaku*, 1954, **26**, 577–579.
46 M. Topsakal, S. Cahangirov, E. Bekaroglu and S. Ciraci, *Phys. Rev. B: Condens. Matter Mater. Phys.*, 2009, **80**, 235119.
47 Y. J. Choi, K. M. Kang and H. H. Park, *Sol. Energy Mater. Sol. Cells*, 2015, **132**, 403–409.
48 J. Vishwakarma, B. Sabu, K. Bhotkar, S. Mehta and H. Muthurajan, *Int. J. Chem. Phys. Sci.*, 2015, **5**, 28–35.
49 F. K. Shan and Y. S. Yu, *J. Eur. Ceram. Soc.*, 2004, **24**, 1869–1872.
50 S. T. Tan, B. J. Chen, X. W. Sun, W. J. Fan, H. S. Kwok, X. H. Zhang and S. J. Chua, *J. Appl. Phys.*, 2005, **98**, 013505.
51 R. Chen, P. Zhu, L. Deng, T. Zhao, R. Sun and C. Wong, *ChemPlusChem*, 2014, **79**, 743–750.
52 B. Liu and H. C. Zeng, *J. Am. Chem. Soc.*, 2003, **125**, 4430–4431.